DOI: 10.61782/fa.2025.0121

FORUM ACUSTICUM
EURONOISE 2025

TOWARDS ANALYTICAL WAVEFORM TRANSITIONS IN SPACE-TIME ACROSS DIFFERENT BOUNDARY CONDITIONS

Elias Zea[1*]
Marcus Wallenberg Laboratory for Sound and Vibration Research, KTH Royal Institute of Technology, Sweden
zea@kth.se

Efren Fernandez-Grande[2]
Department of Audiovisual and Communications Engineering, Technical University of Madrid, Spain
efren.fernandez@upm.es

C. Evren Yarman[3]
Schlumberger Riboud Product Center, France
Department of Mathematics, KTH Royal Institute of Technology, Sweden
cyarman@slb.com

ABSTRACT

This study investigates an analytical framework to parametrize transitions of acoustic waves in space-time. The work considers a linear microphone array and a point source in a linear, non-dispersive medium between two parallel, rigid wall surfaces. The proposed framework parametrizes spatiotemporal waveforms into frequency/phase-speed representations, leveraging the physical attributes of the boostlet transform. The parametrization suggests that a superposition of plane waves boosted along a hyperbola in the Fourier domain resembles the Green's function solution in this two-wall problem. This hyperbola is centered on the frequency axis, and its apex can be related to the distance between the walls. In particular, we find a resemblance between the Gaussian-parametrized waveforms and the Green's function solution. The motivation for this work originates from deriving a framework that easily parametrizes transitions between free and reverberant spaces, offering versatility in modeling local and global spatiotemporal wave propagation phenomena.

Keywords: *waveform transitions, boostlets, space-time, boundary conditions, microphone array processing.*

**Corresponding author: zea@kth.se.*

1. INTRODUCTION

A long-standing challenge in room acoustics is effectively modeling the transition between the free-space propagation of the direct sound and the diffuse, reverberant response that emerges after many reflections [1]. Capturing this transition is non-trivial since the underlying physics involves fundamentally different processes, such as direct sound, early reflections, and late reverberation, including intricate diffraction and scattering phenomena (due to objects, boundaries, etc.) that appear in the room impulse response (RIR). Consequently, accurate input data for boundary conditions, e.g., absorption and scattering coefficients, and their skillful discretization, steer the performance of numerical simulation methods [2]. This polychotomy has motivated hybrid modeling strategies, such as [3, 4]. However, these approaches typically hard-partition the RIR into early and late components rather than providing a unified parametric representation of the continuous transition between the two. A key objective of current research is thus to devise frameworks that effectively and efficiently interpolate between free-field and fully bounded wave propagation in a broadband, physics-grounded manner.

Efficiently analyzing and processing wavefield recordings in enclosures is critical in various applications, such as sound field reconstruction and control, architectural acoustics, virtual reality, and teleconferencing. Over time, room acoustics modeling has progressed from initial geometrical-acoustics methods [5], including ray tracing [6] and the image-source method [7], to increasingly sophisticated numerical and data-driven techniques.

Botteldooren applied the finite-difference-time-domain method to simulate low-frequency room acoustical phenomena [8]. Berkhout *et al.* proposed a wavefield extrapolation approach based on a discretization of the Rayleigh II integral operator and the plane-wave reflection coefficient of the rooms' walls [9]. Discontinuous Galerkin schemes [10] and spectral element methods [11] have also gained recent popularity. Lastly, recent data-driven approaches, such as [12–16], attain impressive results due to their ability to extract the most relevant features to reconstruct the sound field.

The idea of modeling boundary-value data with local solutions in space-time was established with Kaiser's foundational works on wavelet acoustics [17] and Gaussian wave packets [18]. Of similar relevance is the Poincaré wavelet transform by Perel and collaborators [19, 20], which is used to decompose the pressure boundary values in space-time as a superposition of localized waveforms, pulsating with a given frequency and propagating with a given rapidity (i.e., phase speed). While applicable to describing multi-scale wavefronts in boundary-value problems, these ideas had not, until the introduction of boostlet systems [21,22], been explored to model spatiotemporal waves in room acoustics.

In particular, many waves found in real rooms are due to complex reflectors, diffraction, or scattering, which depart from the classical analytical functions used frequently in theoretical, computational, and experimental models. The motivation for this work is to seek an analytical framework that can model complex wave propagation in space-time and to examine whether this framework can account for modeling the transition between sound waves traveling in free space and interacting with the domain boundaries. The proposed framework is based on the mathematical structures common to Poincaré wavelets [19] and boostlets [21], which consist of dilations and boosts in 2D space-time.

The paper is structured as follows. Section 2 describes the Green's function solutions in free space and the presence of rigid walls. Section 3 overviews the framework, built upon Gaussian functions of dilations and boosts and their analytical inverse Fourier transforms. Section 4 includes the key findings and results. Concluding remarks are given in Sec. 5.

2. GREEN'S FUNCTION PRELIMINARIES

Consider the linearized inhomogeneous (3+1)D wave equation in free space with a point source at coordinates $\vec{\mathbf{r}}_0 = (x_0, y_0, z_0)$ emitting a pulse at $t = 0$,

$$\left(\frac{\partial^2}{\partial t^2} - c^2\nabla^2\right) p(t, \vec{\mathbf{r}}) = \delta(t, \vec{\mathbf{r}} - \vec{\mathbf{r}}_0), \tag{1}$$

where $\vec{\mathbf{r}} = (x, y, z) \in \mathbb{R}^3$ denotes the 3D spatial coordinates, $t \in \mathbb{R}^+$ denotes the time coordinate, c is the sound speed, and $\nabla^2 = \partial_{xx} + \partial_{yy} + \partial_{zz}$ is the associated Laplacian. It is well-known that the solution $p(t, \vec{\mathbf{r}})$ is the free-space Green's function

$$G_0(t, \vec{\mathbf{r}}) = \frac{\delta\left(t - \frac{\|\vec{\mathbf{r}} - \vec{\mathbf{r}}_0\|}{c}\right)}{4\pi\|\vec{\mathbf{r}} - \vec{\mathbf{r}}_0\|}, \tag{2}$$

where $\|\vec{\mathbf{r}} - \vec{\mathbf{r}}_0\| = \sqrt{(x - x_0)^2 + (y - y_0)^2 + (z - z_0)^2}$.

Let us now introduce an acoustically-hard planar surface at $z = L/2$, that is, a Neumann boundary condition that vanishes the normal particle velocity at the surface, i.e.,

$$\frac{\partial p(t, \vec{\mathbf{r}})}{\partial z} = 0, \quad \text{at} \quad \vec{\mathbf{r}} = (x, y, L/2). \tag{3}$$

The image-source method can incorporate the above boundary condition into the wave equation. Then, the source term becomes the sum of the source, placed at $\vec{\mathbf{r}}_0$, and its mirrored image, placed at $\vec{\mathbf{r}}_1 = (x_0, y_0, z_0 + L)$. In mathematical terms,

$$\left(\frac{\partial^2}{\partial t^2} - c^2\nabla^2\right) p(t, \vec{\mathbf{r}}) = \delta(t, \vec{\mathbf{r}} - \vec{\mathbf{r}}_0) + \delta(t, \vec{\mathbf{r}} - \vec{\mathbf{r}}_1), \tag{4}$$

which leads to the following Green's function

$$G_1(t, \vec{\mathbf{r}}) = \frac{\delta\left(t - \frac{\|\vec{\mathbf{r}} - \vec{\mathbf{r}}_0\|}{c}\right)}{4\pi\|\vec{\mathbf{r}} - \vec{\mathbf{r}}_0\|} + \frac{\delta\left(t - \frac{\|\vec{\mathbf{r}} - \vec{\mathbf{r}}_1\|}{c}\right)}{4\pi\|\vec{\mathbf{r}} - \vec{\mathbf{r}}_1\|}. \tag{5}$$

Finally, we can add another acoustically rigid wall at $z = -L/2$, i.e., the source is exactly between the two walls. In this case, there are infinitely many reflections, which are then summed to give the source term. In mathematical terms,

$$\left(\frac{\partial^2}{\partial t^2} - c^2\nabla^2\right) p(t, \vec{\mathbf{r}}) = \sum_{n\in\mathbb{Z}} \delta(t, \vec{\mathbf{r}} - \vec{\mathbf{r}}_n), \tag{6}$$

where the spatial coordinates of the n-th source term are given by $\vec{\mathbf{r}}_n = (x_0, y_0, z_0 + nL)$, which yields the Green's function

$$G_\infty(t, \vec{\mathbf{r}}) = \sum_{n\in\mathbb{Z}} \frac{\delta\left(t - \frac{\|\vec{\mathbf{r}} - \vec{\mathbf{r}}_n\|}{c}\right)}{4\pi\|\vec{\mathbf{r}} - \vec{\mathbf{r}}_n\|}. \tag{7}$$

In this paper, we will concentrate on the case of a source located at $\vec{\mathbf{r}}_0 = (0,0,0)$ and a line of receivers located at $\vec{\mathbf{r}} = (x,0,0)$, which reduces the dimensionality of the Green's function to 2D space-time:

$$G_\infty(t,x,0,0) = \sum_{n\in\mathbb{Z}} \frac{\delta\left(t - \frac{\sqrt{x^2+(nL)^2}}{c}\right)}{4\pi\sqrt{x^2+(nL)^2}}. \quad (8)$$

3. ANALYTICAL FRAMEWORK

In the former section, we introduced the basic theory of Green's functions in free space and within two infinite rigid walls. This section will describe the framework using analytical functions parametrized in terms of dilations and boosts, exploiting the mathematical structure of Poincaré wavelets [19] and boostlets [21].

3.1 Frequency-phase-speed representations

Let us define a 2D spatiotemporal function $g(t,x) \in L^2(\mathbb{R}^2)$ by taking its 2D inverse Fourier transform along regions intersected by lines crossing through the origin and hyperbolas in the frequency-wavenumber domain $(\omega, k_x) \in \mathbb{R}^2$. In mathematical terms,

$$g(t,x) = \int_{\mathbb{R}^2} |\alpha|\, g(\alpha,\theta)\, \mathrm{e}^{\mathrm{j}\alpha(t\cosh\theta - x\sinh\theta)}\, \mathrm{d}\alpha\mathrm{d}\theta, \quad (9)$$

where $g(\alpha,\theta) \in L^2(\mathbb{R}^2)$ is a representation of $g(t,x)$ in the frequency/phase-speed domain, $\alpha \in \mathbb{R}^+$ is a dilation parameter representing the frequency, and $\theta \in \mathbb{R}$ is a (Lorentz) boost parameter representing the phase speed $c_x = c\tanh\theta$ along the x axis [23]. Note the change of coordinates $(\omega, k_x) \mapsto (\alpha\cosh\theta, -\alpha\sinh\theta)$ applied to the Fourier basis functions.

It is worth commenting on the physical interpretation of dilations and boosts. Isotropic dilations deform a wave function $g(t,x)$ by shifting its frequency content. In short, dilating by α shrinks or expands the wave function in 2D space-time. Similarly, Lorentz boosts θ perform an anisotropic (hyperbolic) deformation of the wave function by increasing or decreasing its phase speed $c_x \in (-c,c)$ along the x axis.

3.2 Dilating and boosting Gaussians

In this work, we are interested in parametrizing functions of the kind $g(t,x)$ into functions $g(\alpha,\theta)$ by controlling the mean and standard deviations of the (α,θ) parameters. Thus, a reasonable approach is to define $g(\alpha,\theta)$ as a Gaussian function. In what follows, we shall assume that the sound speed is $c = 1$ m/s.

Consider the Gaussian function

$$g(\alpha,\theta;\nu_{\alpha,\theta}) = |\alpha|\, \frac{\mathrm{e}^{-(\alpha-\mu_\alpha)^2/(2\sigma_\alpha^2)}}{\sqrt{2\pi\sigma_\alpha^2}}\, \frac{\mathrm{e}^{-(\theta-\mu_\theta)^2/(2\sigma_\theta^2)}}{\sqrt{2\pi\sigma_\theta^2}}, \quad (10)$$

where $(\mu_\bullet, \sigma_\bullet) \in \mathbb{R}\times\mathbb{R}^+$ are the mean and standard deviations of the $\bullet = \alpha,\theta$ parameters, and we use the notation $\nu_{\alpha,\theta} = (\mu_\alpha, \mu_\theta, \sigma_\alpha, \sigma_\theta)$.

Since g above lives in $L^2(\mathbb{R}^2)$, such a Gaussian is also a continuous boostlet [21] whose support is mean-centered at $(\alpha,\theta) = (\mu_\alpha, \mu_\theta)$ and lives within a standard deviation cell of size $\sigma_\alpha \times \sigma_\theta$. Consequently, it is possible to construct a continuous set of functions using a collection of dilated and boosted Gaussians to decompose and reconstruct spatiotemporal wavefields.

Finally, consider the space-time, integral representation of the Gaussian in Eq. (10) via (9)

$$\begin{aligned} g(t,x;\nu_{\alpha,\theta}) = \int_{\mathbb{R}^2} |\alpha| &\frac{\mathrm{e}^{-(\alpha-\mu_\alpha)^2/(2\sigma_\alpha^2)}}{\sqrt{2\pi\sigma_\alpha^2}} \\ &\times \frac{\mathrm{e}^{-(\theta-\mu_\theta)^2/(2\sigma_\theta^2)}}{\sqrt{2\pi\sigma_\theta^2}} \\ &\times \mathrm{e}^{\mathrm{j}\alpha(t\cosh\theta - x\sinh\theta)}\, \mathrm{d}\alpha\mathrm{d}\theta. \end{aligned} \quad (11)$$

An example of such a Gaussian in the Fourier and (α,θ) domains is depicted in Fig. 1 below.

4. KEY FINDINGS

We are now equipped to consider two special cases of the integral expression in Eq. (11) by taking limits of the standard deviations σ_α and σ_θ.

4.1 Special case 1: Harmonic plane waves

This case has been identified previously in [21], and follows when the standard deviations of the dilation and boost parameters $(\sigma_\alpha, \sigma_\theta)$ both tend to zero, $\nu_{\alpha,\theta} = (\mu_\alpha, \mu_\theta, 0, 0)$:

$$\begin{aligned} \lim_{\substack{\sigma_\alpha\to 0\\ \sigma_\theta\to 0}} g(t,x;\nu_{\alpha,\theta}) = \int_{\mathbb{R}^2} &\exp\left(\mathrm{j}\alpha\left[t\cosh\theta - x\sinh\theta\right]\right) \\ &\times \delta\left(\alpha-\mu_\alpha, \theta-\mu_\theta\right) |\alpha|\, \mathrm{d}\alpha\mathrm{d}\theta, \end{aligned} \quad (12)$$

which collapses the Gaussian function into a Dirac delta mean-centered at $(\alpha,\theta) = (\mu_\alpha, \mu_\theta)$. In this case, we re-

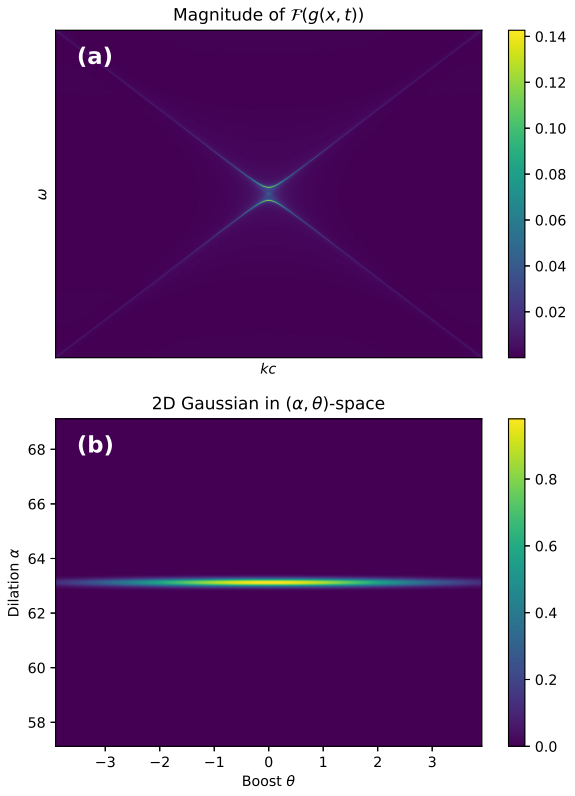

Figure 1. 2D Gaussian function $g(t, x; \nu_{\alpha,\theta})$ with parameters $\nu_{\alpha,\theta} = \left(20\pi, 0, 0, \cosh^{-1}(25)\right) \approx (62.83, 0, 0, 3.91)$. (a) Gaussian in the Fourier domain. (b) Gaussian in the dilation-boost domain. The function depicted in (a) is obtained via Eq. (14). The mapping between (a) and (b) is dictated by the hyperbolic change of coordinates $(\alpha(k,\omega), \theta(k,\omega))$.

cover

$$g(t, x; \nu_{\alpha,\theta}) = |\mu_\alpha| \exp\left(\mathrm{j}\mu_\alpha \left[t\cosh\mu_\theta - x\sinh\mu_\theta\right]\right), \tag{13}$$

which behaves like a plane wave with frequency $\omega = \mu_\alpha$ and phase speed $c_x = \tanh(\mu_\theta)$ inside the causality cone.

An example of such a function is plotted in Fig. 2 with mean dilation (i.e., angular frequency of normal-incident waves) $\mu_\alpha = 6\pi$ rad/s, i.e., 3 Hz. The plane wave oscillates around 6 times on the positive (conversely, negative) time interval considered (here ± 1 seconds). This comes from the fact that the mean boost $\mu_\theta = 1$ rad increases the number of oscillations hyperbolically, approximately by a factor of $\cosh(\mu_\theta) \approx 1.5$ in this case. We find the wavefront distortions on the upper-right (conversely, lower-left) cone boundary $t = x/c$ peculiar and requiring further investigation.

4.2 Special case 2: Harmonic spherical waves

Another special case is obtained when the standard deviation of the dilation parameter $\sigma_\alpha \to 0$, i.e., $\nu_{\alpha,\theta} = (\mu_\alpha, 0, 0, \sigma_\theta)$. This is equivalent to a hyperbola in Fourier space whose apex is governed by the mean dilation μ_α. An example of such a function is plotted in Fig. 3 with mean angular frequency (of normal-incident waves) $\mu_\alpha = 20\pi$ rad/s, i.e., 10 Hz. These oscillations can be observed in the gradually decaying wavefronts along the positive (conversely, negative) time axis.

Without loss of generality, let us assume the mean boost $\mu_\theta = 0$ in what follows and take the limit

$$\begin{aligned}\lim_{\sigma_\alpha\to 0} g(t, x; \nu_{\alpha,\theta}) = &\exp\left[\mathrm{j}\mu_\alpha\sqrt{t^2-x^2}\left(1+\frac{\theta_0^2}{2}\right)\right] \\ &\times \exp\left[-\frac{1}{2}\frac{\sigma_\theta^2\left(\theta_0\sqrt{t^2-x^2}\right)^2\mu_\alpha^2}{1-\mathrm{j}\mu_\alpha\sigma_\theta^2\sqrt{t^2-x^2}}\right] \\ &\times \frac{|\mu_\alpha|}{\sqrt{1-\mathrm{j}\mu_\alpha\sigma_\theta^2\sqrt{t^2-x^2}}},\end{aligned} \tag{14}$$

where $\theta_0 = \operatorname{arctanh}(x/t)$ is the stationary point of the phase of the Fourier basis in Eq. (11), obtained as θ for which

$$\frac{\partial}{\partial\theta}\left[t\sinh\theta - x\cosh\theta\right] = 0. \tag{15}$$

As depicted in Fig. 3(a) and (d), the real and imaginary parts of $\lim_{\sigma_\alpha\to 0} g(t, x; \nu_{\alpha,\theta})$ in Eq. (14) are hyperbolic and are supported within the causality cone. In particular, the imaginary (and likewise real) part of $\lim_{\sigma_\alpha\to 0} g(t, x, \nu_{\alpha,\theta})$ has zeros at (t, x) satisfying

$$(t^2-x^2)\left[1+\frac{\theta_0^2}{2}-\frac{1}{2}\frac{\sigma_\theta^4(t^2-x^2)\theta_0^2\mu_\alpha^2}{1+\mu_\alpha^2\sigma_\theta^4(t^2-x^2)}\right] = \left(\frac{n\pi}{\mu_\alpha}\right)^2, \tag{16}$$

for $n \in \mathbb{Z}$. Expanding the standard deviation of the boost $\sigma_\theta \to \infty$ gives

$$\lim_{\sigma_\theta\to\infty}(t^2-x^2)\left(1+\frac{\theta_0^2}{2}-\frac{\theta_0^2}{2}\right)^2 = t^2-x^2 = \left(\frac{n\pi}{\mu_\alpha}\right)^2, \tag{17}$$

for $n \in \mathbb{Z}$, equivalent to a set of hyperbolic wavefronts with apexes $(n\pi/\mu_\alpha)^2$.

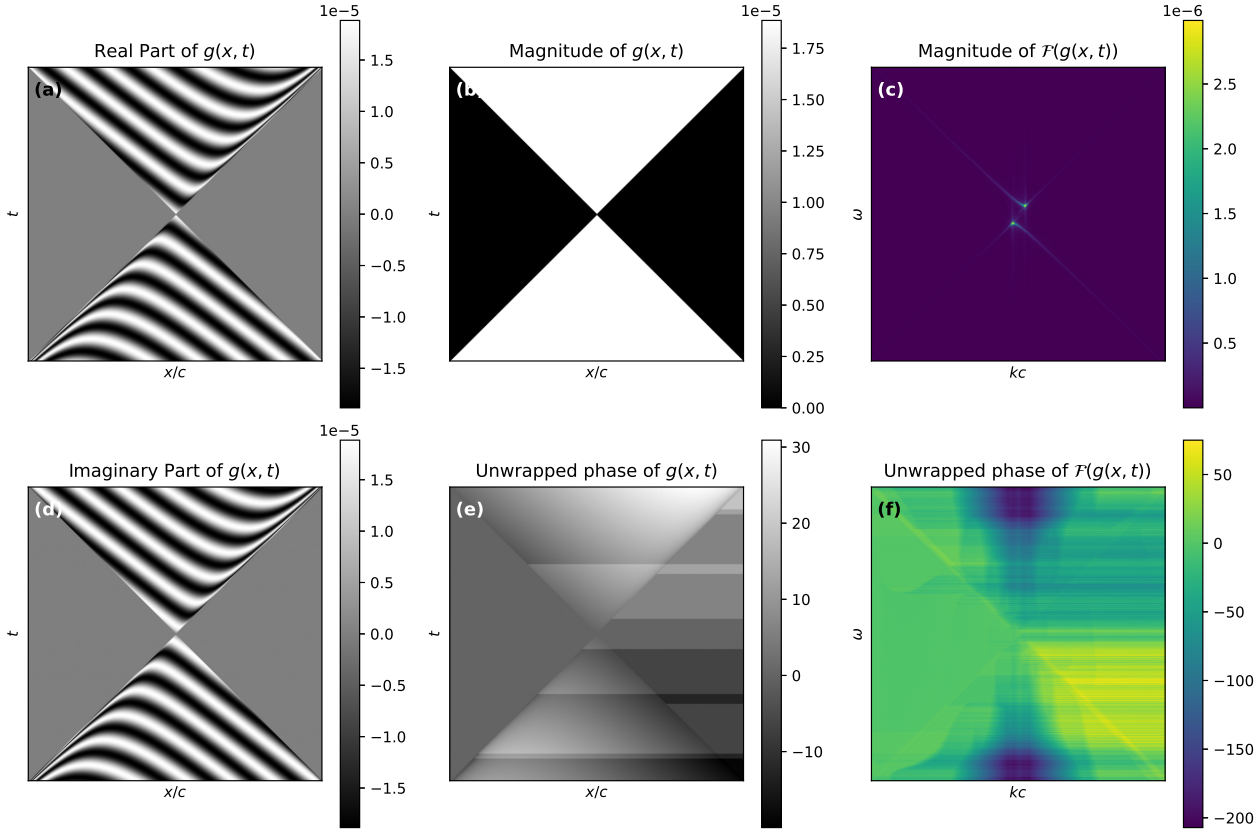

Figure 2. Harmonic, plane wave-like, Gaussian-boostlet function $g(x, t; \nu_{\alpha,\theta})$ computed via Eq. (13), mean-centered at $(\mu_\alpha, \mu_\theta) = (6\pi \text{ rad/s}, 1 \text{ rad})$, and (theoretically) infinitesimally small boost and dilation standard deviations, $\sigma_\alpha, \sigma_\theta \to 0$. (a) Real and (d) imaginary parts in space-time. (b) Magnitude and (e) phase in space-time. Fourier transform (c) magnitude and (f) phase.

4.3 Resemblance to $G_\infty(t, x, 0, 0)$

Suppose we set the mean dilation $\mu_\alpha = \pi/L$ according to the distance between the two rigid walls L and fix the source's excitation frequency to $\omega = \mu_\alpha$. In that case, we find that this set of points is the same as those supporting the Green's function $G_\infty(t, x, 0, 0)$ in Eq. (7), i.e., when the receivers are placed at $\vec{r} = (x, 0, 0)$, and the source is placed at $\vec{r}_s = (0, 0, 0)$. Although this does not provide direct evidence of an approximation of $G_\infty(t, x, 0, 0)$, it indicates that its peaks match exactly with the maxima of

$$\lim_{\substack{\sigma_\alpha \to 0 \\ \sigma_\theta \to \infty}} g(t, x; \nu_{\alpha,\theta}). \tag{18}$$

Let us analyze the above Gaussian $g(t, x; \nu_{\alpha,\theta})$ at a fixed location in space. Figure 4 shows the real and imaginary parts, as well as the magnitude and phase of $g(t, x_{\text{loc}}; \nu_{\alpha,\theta})$ in Fig. 3, i.e., evaluated at $x = x_{\text{loc}} = 0.5$ m plotted against time. The real and imaginary parts show the ten oscillations corresponding to the mean dilation. The magnitude and phase have an onset at $t = x_{\text{loc}}$. These onsets can be approximated by a Heaviside function $H(t - x_{\text{loc}}/c)$. The amplitude decay of the onset is overlaid with the hyperbolic function $1/\sqrt{t^2 - x_{\text{loc}}^2}$, which corresponds to the inverse distance in 2D Minkowski space. Similarly, the phase after the Heaviside onset is overlaid with the hyperbolic function $\mu_\alpha \sqrt{t^2 - x_{\text{loc}}^2}$. Further investigation is needed to understand the source term characteristics that lead to the waveforms $g(t, x; \nu_{\alpha,\theta})$.

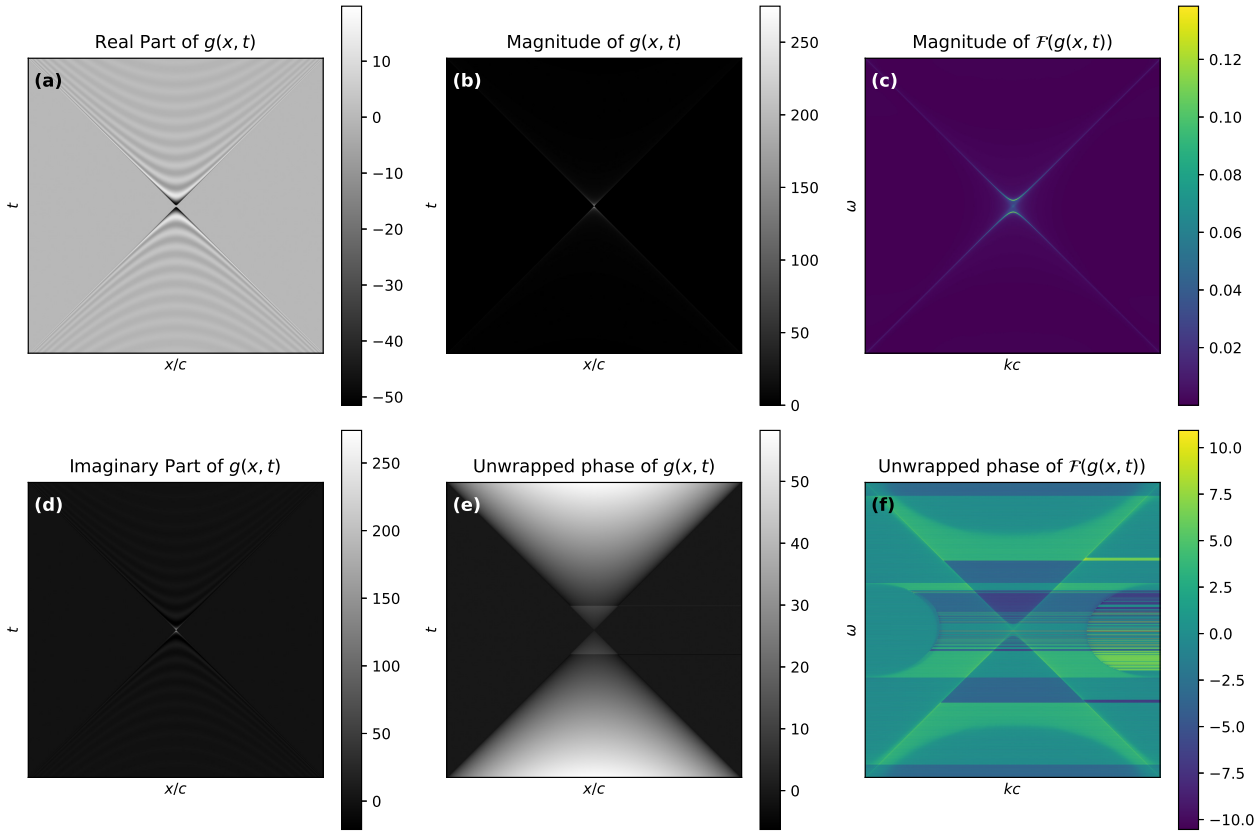

Figure 3. Harmonic, spherical wave-like, Gaussian-boostlet function $g(x,t;\nu_{\alpha,\theta})$ computed via Eq. (14), mean-centered at $(\mu_\alpha,\mu_\theta) = (20\pi \text{ rad/s}, 0 \text{ rad})$, and with (theoretically) infinite boost standard deviation, $\sigma_\theta \to \infty$, and infinitesimally small dilation standard deviation, $\sigma_\alpha \to 0$. (a) Real and (d) imaginary parts in space-time. (b) Magnitude and (e) phase in space-time. Fourier transform (c) magnitude and (f) phase..

5. CONCLUDING REMARKS

The Green's function solution of a point source between two parallel rigid walls demonstrates a certain resemblance to analytical parametrizations of Guassians with *narrowband* frequency content and *broadband* phase-speed content. Follow-up research will focus on the two remaining limits of standard deviations in the Gaussians, that is, $(\sigma_\alpha,\sigma_\theta) \to (\infty,0)$ and $(\sigma_\alpha,\sigma_\theta) \to (\infty,\infty)$. These cases suggest a correspondence with transient planar waves—i.e., *broadband* frequency content and *narrowband* phase-speed content—and transient spherical waves—i.e., *broadband* frequency and phase-speed content. Transitions between the four wave shapes are suspected to parametrize damping and spherical spreading.

6. ACKNOWLEDGMENTS

E.Z. is financially supported by the Swedish Research Council, grant No. 2020-04668. Thanks to Marco Laudato and Joakim Andén, who have greatly contributed to the ideas explored in this paper.

7. REFERENCES

[1] L. Savioja and U. P. Svensson, "Overview of geometrical room acoustic modeling techniques," *J. Acoust. Soc. Am.*, vol. 138, no. 2, pp. 708–730, 2015.

[2] M. Vorländer, "Computer simulations in room acoustics: Concepts and uncertaintiesa)," *J. Acoust. Soc. Am.*, vol. 133, pp. 1203–1213, 03 2013.

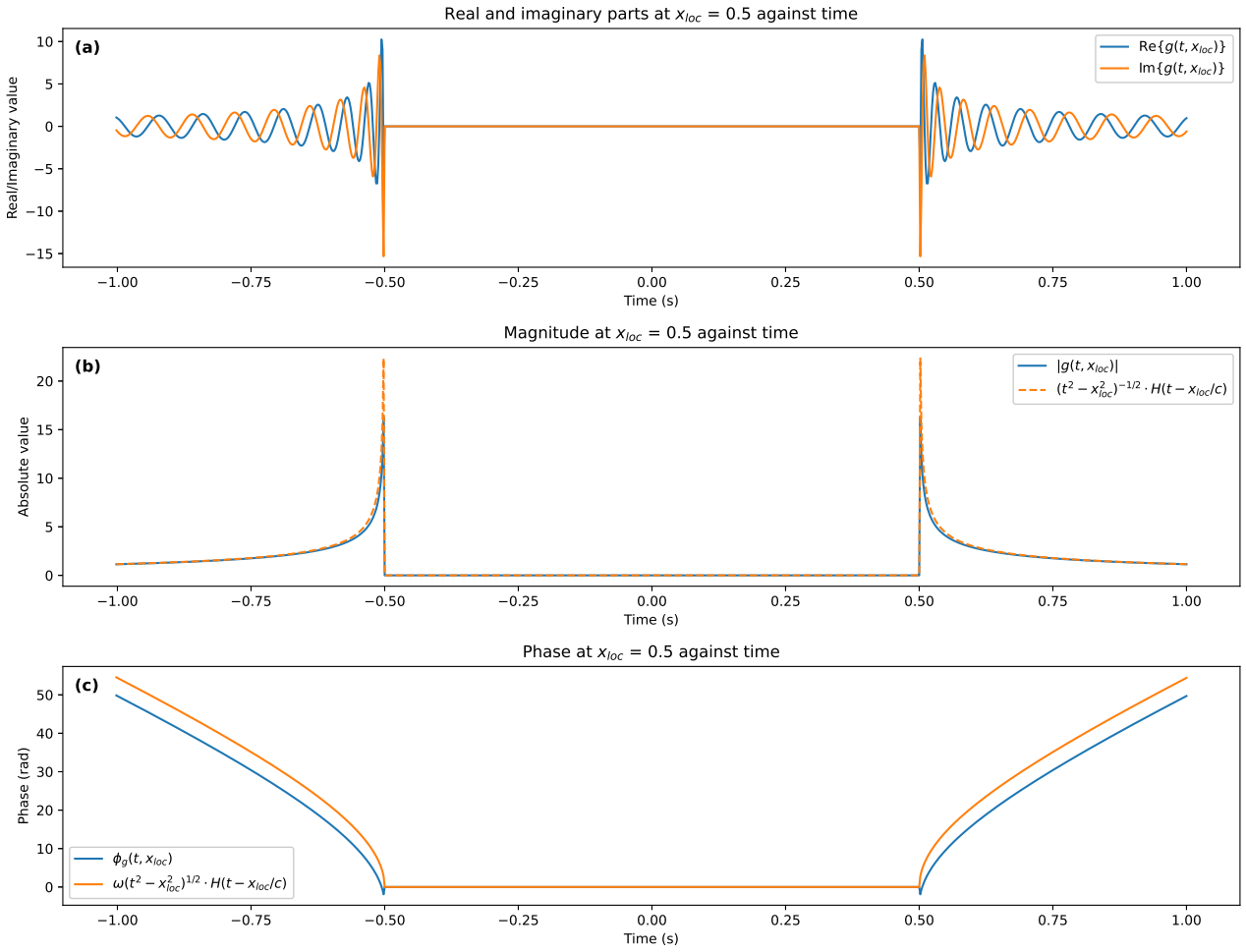

Figure 4. (a) Real and imaginary parts, (b) magnitude, and (c) phase of the Gaussian-boostlet function computed via Eq. (14) evaluated at $x = x_{\mathrm{loc}}$ plotted against time.

[3] A. Southern, S. Siltanen, D. T. Murphy, and L. Savioja, "Room impulse response synthesis and validation using a hybrid acoustic model," *IEEE Transactions on Audio, Speech, and Language Processing*, vol. 21, no. 9, pp. 1940–1952, 2013.

[4] G. I. Koutsouris, J. Brunskog, C.-H. Jeong, and F. Jacobsen, "Combination of acoustical radiosity and the image source method," *J. Acoust. Soc. Am.*, vol. 133, pp. 3963–3974, 06 2013.

[5] M. R. Schroeder, B. S. Atal, and C. Bird, "Digital computers in room acoustics," in *Proc. 4th ICA, Copenhagen M*, vol. 21, 1962.

[6] A. Krokstad, S. Strøm, and S. Sørsdal, "Calculating the acoustical room response by the use of a ray tracing technique," *J. Sound Vib.*, vol. 8, no. 1, pp. 118–125, 1968.

[7] J. Allen and D. Berkley, "Image method for efficiently simulating small-room acoustics," *J. Acoust. Soc. Am.*, vol. 65, pp. 943–950, 1979.

[8] D. Botteldooren, "Finite-difference time-domain simulation of low-frequency room acoustic problems," *J. Acoust. Soc. Am.*, vol. 98, no. 6, pp. 3302–3308, 1995.

[9] A. J. Berkhout, D. de Vries, J. Baan, and B. W. van den Oetelaar, "A wave field extrapolation ap-

proach to acoustical modeling in enclosed spaces," *J. Acoust. Soc. Am.*, vol. 105, no. 3, pp. 1725–1733, 1999.

[10] H. Wang, I. Sihar, R. Pagán Muñoz, and M. Hornikx, "Room acoustics modelling in the time-domain with the nodal discontinuous Galerkin method," *J. Acoust. Soc. Am.*, vol. 145, pp. 2650–2663, 04 2019.

[11] F. Pind, A. P. Engsig-Karup, C.-H. Jeong, J. S. Hesthaven, M. S. Mejling, and J. Strømann-Andersen, "Time domain room acoustic simulations using the spectral element method," *J. Acoust. Soc. Am.*, vol. 145, pp. 3299–3310, 06 2019.

[12] X. Karakonstantis and E. Fernandez-Grande, "Generative adversarial networks with physical sound field priors.," *J. Acoust. Soc. Am.*, vol. 154, pp. 1226–1238, Aug 2023.

[13] E. Fernandez-Grande, X. Karakonstantis, D. Caviedes-Nozal, and P. Gerstoft, "Generative models for sound field reconstruction," *J. Acoust. Soc. Am.*, vol. 153, pp. 1179–1190, 02 2023.

[14] N. Borrel-Jensen, S. Goswami, A. P. Engsig-Karup, G. E. Karniadakis, and C.-H. Jeong, "Sound propagation in realistic interactive 3D scenes with parameterized sources using deep neural operators," *Proc. Natl. Acad. Sci. U.S.A.*, vol. 121, no. 2, p. e2312159120, 2024.

[15] X. Karakonstantis, D. Caviedes-Nozal, A. Richard, and E. Fernandez-Grande, "Room impulse response reconstruction with physics-informed deep learning," *J. Acoust. Soc. Am.*, vol. 155, no. 2, pp. 1048–1059, 2024.

[16] S. Olivieri, M. Pezzoli, F. Antonacci, and A. Sarti, "Physics-informed neural network for volumetric sound field reconstruction," *EURASIP J. Audio Speech Music. Process.*, vol. 2024, no. 1, pp. 1–17, 2024.

[17] G. Kaiser, *Wavelet Acoustics*, pp. 271–290. Boston: Birkhäuser Boston, 2011.

[18] A. Kiselev and M. Perel, "Gaussian wave packets," *Optics and Spectroscopy*, vol. 86, no. 3, pp. 357–359, 1999.

[19] M. V. Perel, "Integral representation of solutions of the wave equation based on Poincaré wavelets," in *Proceedings of the International Conference Days on Diffraction 2009*, pp. 159–161, 2009.

[20] M. V. Perel and E. A. Gorodnitskiy, *Decomposition of Solutions of the Wave Equation into Poincaré Wavelets*, pp. 343–352. Cham: Springer International Publishing, 2019.

[21] E. Zea, M. Laudato, and J. Andén, "A continuous boostlet transform for acoustic waves in space-time," *arXiv preprint arXiv:2403.11362*, 2024.

[22] E. Zea, M. Laudato, and J. Andén, "Sparse wavefield reconstruction and denoising with boostlets," in *International Conference on Sampling Theory and Applications (SampTA)*, 2025.

[23] E. G. Williams, *Fourier Acoustics: Sound Radiation and Nearfield Acoustical Holography*. San Diego: Academic Press, 1999.